ELSEVIER

Earth and Planetary Science Letters 199 (2002) 429–445

EPSL

www.elsevier.com/locate/epsl

PKP travel times at near antipodal distances: implications for inner core anisotropy and lowermost mantle structure

Xinlei Sun *, Xiaodong Song

Department of Geology, University of Illinois, Urbana, IL 61801, USA

Received 27 December 2001; revised 4 March 2002; accepted 7 March 2002

Abstract

Previous studies from PKP(AB–DF) differential travel times at large distances suggest that the central part of the inner core is very anisotropic. These differential times, however, can be affected greatly by strong heterogeneity in the lowermost mantle. Here we examine a unique data set of PKP travel times from global digital and analog stations at near antipodal distances, where the effects of both inner core anisotropy and mantle heterogeneity are the greatest. Our results show that the AB–DF residuals for the polar paths are consistently larger than those of the equatorial paths by over 3–4 standard deviations. We also measured DF and AB absolute times, and found that the DF residuals are negatively correlated with the AB–DF residuals while the AB residuals have a much weaker correlation with the AB–DF residuals. We compare several mantle models with the data. Our results suggest that the mantle structure can explain part of the residuals of the equatorials paths, but cannot explain the polar path anomalies. These results strongly suggest that most of the AB–DF anomalies for the polar paths are likely from the inner core anisotropy and not from mantle heterogeneity. Assuming a uniform cylindrical anisotropy model, the average inner core anisotropy amplitude is about 2.5%. On the other hand, equatorial paths from events in the west Pacific and recorded at South America show a steep azimuthal change in AB–DF times (about 4 s over a 60° azimuthal range). The sharp change is well predicted by existing P and S tomographic models: the azimuthal change occurs as the AB paths sweep across the great slow anomaly in the central Pacific. The high correlation between the P and S velocities suggests that the central Pacific slow anomaly may be of thermal origin.

Keywords: PKP-waves; inner core; anisotropy; lower mantle; Central Pacific

1. Introduction

The inner core is dominated by cylindrical anisotropy with the axis of symmetry aligned approximately with the NS spin axis [1,2]. Compressional P waves traversing the inner core in the NS direction are about 3% faster than those in EW directions (for recent reviews, see [3–6]). The anisotropy is likely the result of preferred alignment of hexagonal close-packed iron crystals in the inner core [7–12]. The mechanism for such preferred alignment is under debate. Proposed mechanisms

* Corresponding author.
Tel.: +1-217-244-7133; Fax: +1-217-244-4996.
E-mail addresses: xsun@uiuc.edu (X. Sun), xsong@uiuc.edu (X. Song).

0012-821X/02/$ – see front matter
PII: S0012-821X(02)00580-0

include: (1) alignment arising from large-scale convective flow in the inner core [13–15], and (2) alignment established during the solidification of iron crystals at the surface of the inner core [16,17]. Accurate models of inner core anisotropy are also important in constraining the rotation of the inner core [18–20]. Thus inner core anisotropy has become an important tool to understand the structure, composition, evolution and dynamics of the Earth's core.

An intriguing picture of a three-dimensional inner core structure has recently started to emerge. The inner core structure appears to vary laterally and with depth. The very top 100–200 km of the inner core appears to be isotropic [21–25], but significant anisotropy (some 3%) seems to persist to the center of the inner core [26,27]. A new inner core seismic triplication was identified, providing direct evidence for a transition from isotropy to anisotropy in the inner core [23,28]. The thickness of the upper isotropic layer may vary from 100–250 km in the western hemisphere to over 400 km in the eastern hemisphere [4,23,28,29]. The western hemisphere is much more anisotropic averaged over the top few hundred kilometers of the inner core than the eastern hemisphere [30,31]. The top 100 km of the inner core, while isotropic, appears to be faster in the eastern hemisphere than in the western hemisphere [24]. So far, two seismological data sets have been used to study the inner core: anomalous splitting of normal modes (e.g. [32]), and anomalous travel times of the waves penetrating the inner core, PKP(DF). Fig. 1A shows the ray paths of various branches of PKP waves and Fig. 1B shows PKP travel time curves. The PKP branches include AB (which turns at the mid-outer core), BC (which turns at the bottom of the outer core), CD (which is reflected from the inner core boundary, also known as PKiKP), and DF (which transverses the inner core). At distances from about 128° to 140°, distinct DF and CD arrivals can be seen in short-period (1 s) records. At about 147° to 155°, there are three arrivals, DF, BC (or diffraction off the C-cusp), and AB. At 140° to 147° near the B-caustic, individual phases are hard to distinguish and only waveforms can be used. At distances beyond about 155°, only DF and and AB branches are observable. Because these ray paths are similar in the mantle, differential travel times between PKP branches are often used to reduce the effect of mantle heterogeneity.

Most inner core studies focus on the shallow part of the inner core using PKP waveforms or differential CD–DF times or BC–DF times. The mantle biases on these differential times are expected to be small because their ray paths are very close together throughout the mantle, although Bréger et al. [33] argues in favor of an important contribution from mantle heterogeneity to the observed BC–DF time anomalies along NS paths, which are attributed to the inner core anisotropy by other studies. To sample the deeper part of (and thus the whole) inner core, we need to use DF arrival times or differential AB–DF times at distances beyond 160°. Normal mode data are not helpful in this case as the modes lose sensitivity to the innermost part of the inner core. Significant anisotropy appears to extend to the center of the Earth from AB–DF times at near antipodal distances [26,27]. However, AB–DF times are influenced by structures both in the inner core and in the lowermost mantle. They are separated by a few thousand kilometers at the core–mantle boundary (CMB). In particular, the AB paths graze the CMB, so the effect of lowermost mantle heterogeneity on the AB phase could be very large. Bréger et al. [34] analyzed a global dataset of AB–DF travel times residuals and concluded that a large part of the signal for polar paths could be explained by deep mantle structure. Thus, the effects of deep mantle structure on AB–DF travel times should be carefully considered in order to reliably estimate the anisotropic structure of the central part of the inner core.

In this study, we assemble and analyze systematically a unique set of PKP data at near antipodal distances. Our goal is to test the influence of lowermost mantle structure and to constrain the degree of the anisotropy in the bulk of the inner core, by examining differential and absolute DF and AB times. The advantages of using PKP waves at near antipodal distances include the following. (1) The effect of inner core anisotropy on DF travel time is greatest as the DF ray travels

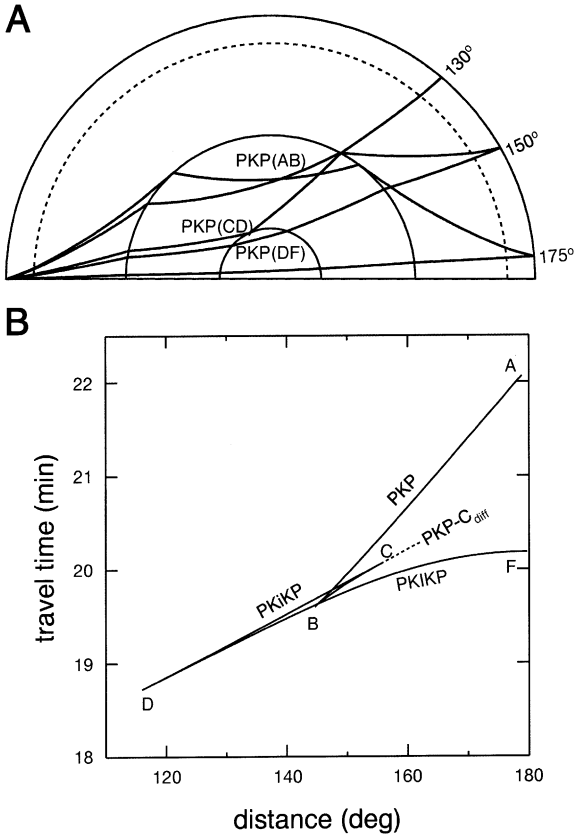

Fig. 1. (A) PKP ray paths at selected distances. (B) PKP travel time curves.

the longest path in the inner core. (2) The effect of lowermost mantle heterogeneity on AB–DF time is greatest because of the largest separation of the two rays. (3) Antipodal waves have the peculiarity that a small variation of source or receiver locations can produce a wide azimuthal coverage of ray paths in the globe [35]. As an extreme example, ray paths from a source, at the north pole to a station at the south pole would cover all the longitudes. Thus, even a limited number of stations that are at near antipodal distances to a few active source regions may result in a good ray coverage.

2. Data

We systematically searched digital data for the period from 1970s to 2000 from stations of Incorporated Research Institutions for Seismology (IRIS), GEOSCOPE, and Program for the Array Seismic Studies of the Continental Lithosphere (PASSCAL). We use vertical components of broadband (BB) or short-period (SP) (if BB channels are not available) records. We also include antipodal data from previous studies: (1) data from Poupinet et al. [35] (courtesy of A. Souriau) and Vinnik et al. [26] (courtesy of B. Romanowicz), which come from analog and digital stations of GEOSCOPE; and (2) data from Song [27], which come from the Global Digital Seismograph Network (GDSN), the Network of Autonomously Recording stations (NARS), and World-Wide Seismograph Station Network (WWSSN) film chips at Lamont-Doherty Earth Observatory. The epicentral distances of our data range from 168° to 180°.

We use a waveform cross-correlation method to measure the AB–DF differential times. The DF waveform is correlated with the AB waveform after correcting the Hilbert transform in the AB waveform. The cross-correlation coefficients of the selected AB–DF differential times are greater than 0.5. Whenever possible, we also pick absolute arrival times. The DF arrival time is picked first and the AB arrival time is inferred from the differential AB–DF time and the DF arrival time. We divide the absolute travel times in three categories: (1) excellent quality: both DF and AB phases are clear and the background noise level is low; (2) good quality: the noise level is moderate and we are confident on the arrival time picks; (3) fair quality: the noise level is high and there may be significant errors of up to about 1 s in the arrival time picks. We sometimes convert BB seismograms to short-period WWSSN seismograms before arrival time picks, if the conversion reduces the noise level.

Finally we obtained 638 AB–DF differential travel time measurements and 470 DF, 466 AB absolute travel time measurements. Fig. 2 shows cross points of the DF and AB rays of all the AB–DF data at the CMB. Although often sparse and not uniform, the ray coverage of the AB rays at the CMB is quite good, with data at all latitudes and longitudes. Note that because the DF rays

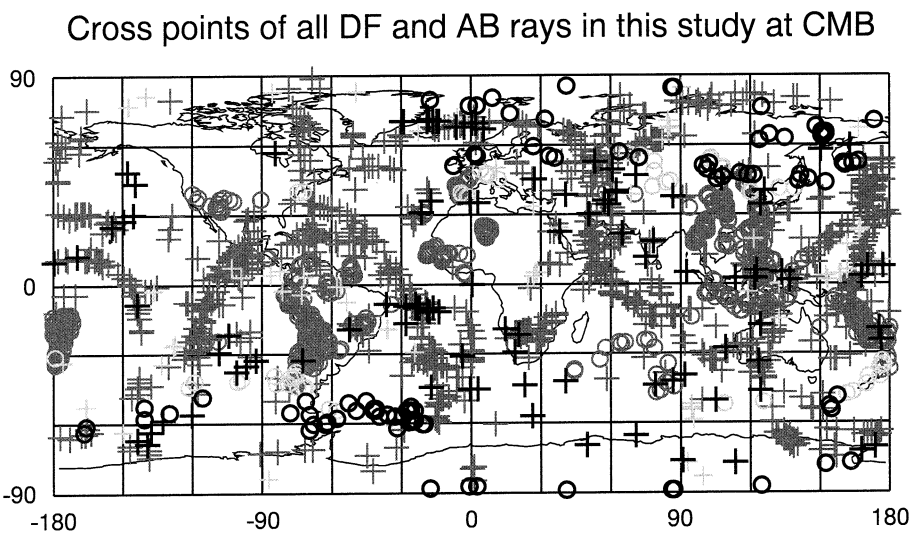

Fig. 2. Cross points at the CMB of all the antipodal PKP rays in this study. Circles and crosses are DF and AB cross points, respectively. The gray scale of the symbols represent cross points from equatorial (gray), polar (dark), and other paths (light), respectively. Note that because DF rays are nearly vertical, DF cross points roughly represent the locations of sources and stations.

are nearly vertical, the DF cross points roughly represent the locations of sources and stations.

Among all the data used, the data newly obtained in this study are 404 AB–DF, 360 DF, and 360 AB measurements; the rest of the data are from previous studies. Of the 470 absolute travel time picks, the numbers of picks that are of excellent, good, and fair quality are 104 (or 22%), 219 (47%), and 33 (7%), respectively. The rest of the DF picks, 114 (24%) (from Poupinet et al. [35]), have no data quality information.

Not surprisingly, most of the data are from equatorial paths. Unless otherwise noted, we refer to those paths whose ray angles with the spin axis at the inner core (ξ) are greater than 50° as equatorial paths in this study. The most important data for studying inner core anisotropy are from polar paths ($\xi < 40°$ unless otherwise noted). We have 60 differential AB–DF measurements from polar paths and for 48 polar paths, we have both absolute DF and AB arrival time picks and differential AB–DF measurements. Of the 48 DF picks, 85% of the data are excellent or good quality data and the rest are fair quality data.

3. Results

3.1. Inner core anisotropy

Fig. 3 shows all the data in the study. Plotted are the travel time residuals relative to the Preliminary Reference Earth Model (PREM) [36] versus the DF ray angle with the spin axis (ξ) for AB–DF (top), DF (middle) and AB (bottom). The dashed lines for the DF and AB absolute travel time residuals (Fig. 3, middle and bottom panels) are the averages of the residuals for equatorial paths with $\xi = 60$ to 90°, which are 3.22 ± 1.55 s and 3.71 ± 1.73 s, respectively (all the errors cited in this paper are one standard deviation (S.D.)). The averages are somewhat different from the PREM baseline corrections for DF and AB (2.18 s and 4.22 s, respectively), but the differences are within the one standard errors. The average of AB–DF residuals for equatorial paths with $\xi = 60$ to 90° is 0.63 ± 1.19 s.

Clearly, AB–DF residuals of the polar paths are anomalously large compared with those of the equatorial paths. The averages of the residuals at $\xi = 0$–10° and $\xi = 0$–30° are 6.01 ± 1.53 s and

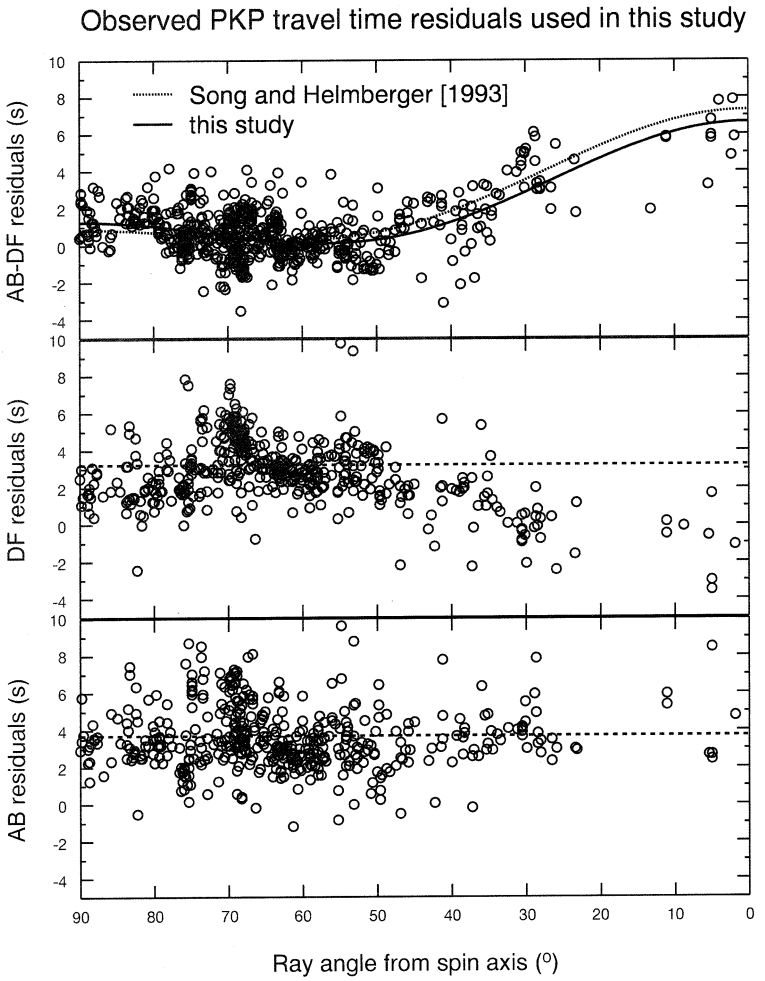

Fig. 3. Travel time residuals relative to PREM [36] versus the angle of the DF leg in the inner core from the spin axis (ξ). (A) Residuals of AB–DF differential times. Assuming a model of uniform anisotropy in the inner core with symmetry around the spin axis, we obtained a least squares model with 2.5% anisotropy amplitude (solid line). The dotted line is the anisotropy model from Song and Helmberger [37] with 3% anisotropy averaged over the top 500 km of the inner core. (B) Residuals of DF absolute times. The dashed line is the average of the DF residuals of the equatorial paths with $\xi > 60°$. Note the DF rays for the polar paths are anomalously fast relative to equatorial paths. (C) The same as B, but for the AB residuals. Note the AB residuals for the polar paths do not appear anomalous.

4.63 ± 1.77 s, respectively. These averages exceed the average of the residuals at $\xi = 60$–$90°$ by 4.5 and 3.4 S.D., respectively. The anomalies appear to be anti-correlated with the corresponding DF residuals and do not have obvious correlation with the corresponding AB residuals (Fig. 3). This suggests that the anomalous AB–DF residuals for the polar paths come mainly from the DF arrivals, which in turn suggests that the anomalies are likely from inner core anisotropy rather than mantle heterogeneity. We will explore this issue later.

If we assume all of the polar path anomalies come from the inner core anisotropy, we can infer the degree of the anisotropy by fitting a cylindrical anisotropy model to all the AB–DF residuals (e.g. [3]). Assuming the anisotropy is uniform throughout the inner core with the fast axis in the NS direction, the fitted cylindrical anisotropy curve is shown by the solid curve of Fig. 3 with

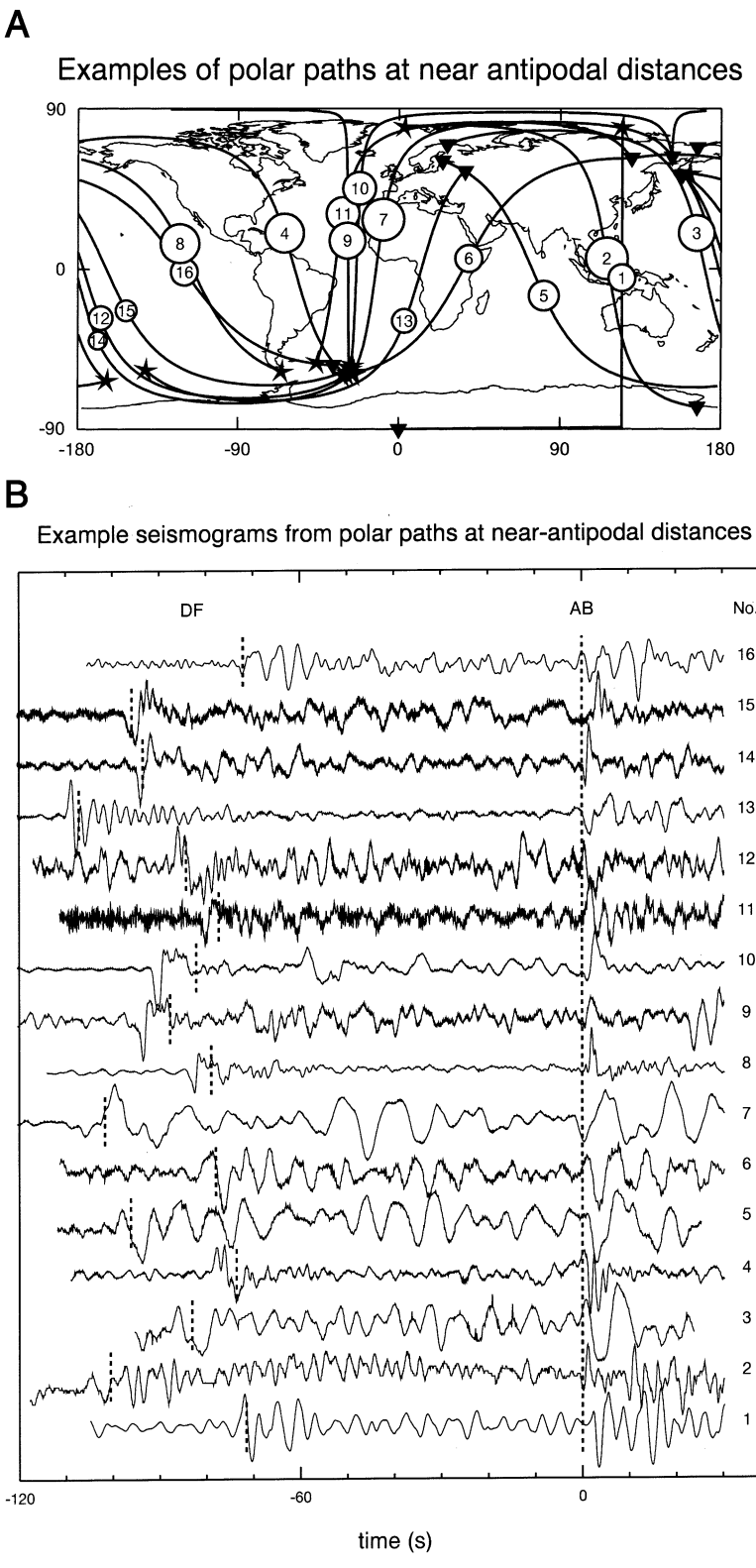
A
Examples of polar paths at near antipodal distances
90
0
-90
-180
-90
0
90
180
B
Example seismograms from polar paths at near-antipodal distances
DF
AB
No.
16
15
14
13
12
11
10
9
8
7
6
5
4
3
2
1
-120
-60
0
time (s)

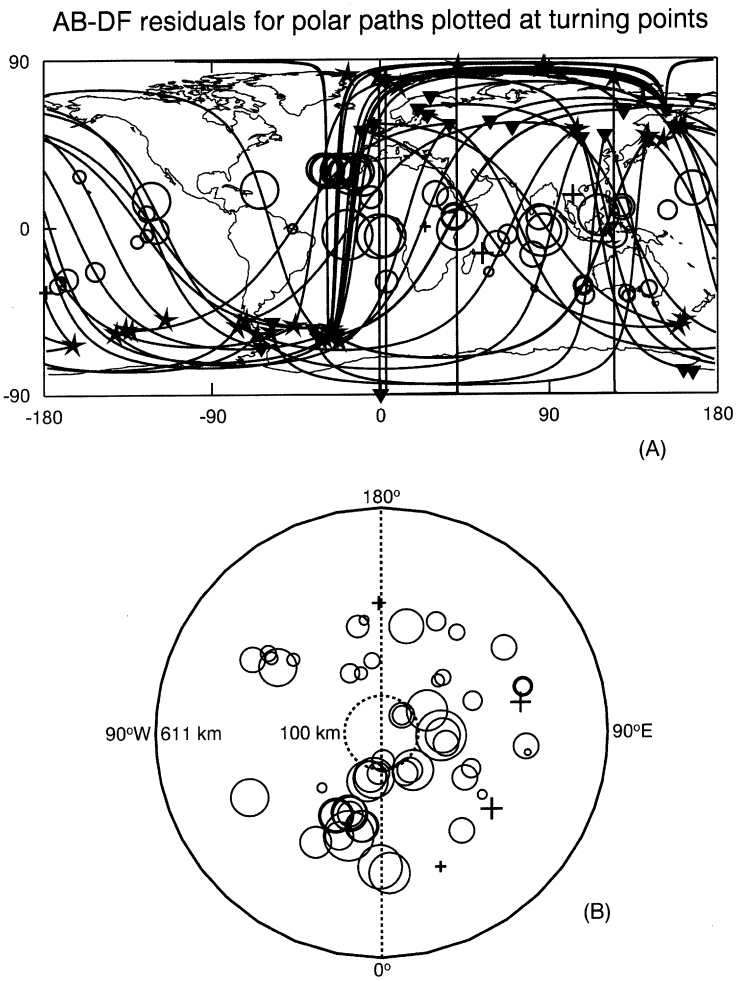

Fig. 5. All the AB–DF residuals for the polar paths plotted at the DF ray turning points in the inner core. (A) Lines are surface projections of the polar ray paths; circles represent positive residuals while crosses represent negative residuals. The symbol sizes are proportional to the anomaly sizes. (B) The radius and the longitude of a turning point are represented by the radius and the angle from bottom measured counterclockwise, respectively. The outer circle is one half of the inner core radius.

the amplitude of the anisotropy 2.5%. This simple model reduces the variance of the polar path data by 50%. The depth extent of the anisotropy can only be roughly constrained with the antipodal data. Assuming the anisotropy amplitudes averaged over the top 500 km of the inner core in the western hemisphere and in the eastern hemisphere are 3.0% ([37], dotted line) and 0.5%

←

Fig. 4. Example data from polar paths at near antipodal distances. (A) The ray paths of selected polar paths. The earthquakes and stations are marked by stars and inverted triangles, respectively. The paths are numbered according to their ray angles with the spin axis (ξ) and are labeled at the turning points of the paths in the inner core. The ray angles range from 5° (path 1) to 36° (path 16). The AB–DF residuals for all these polar paths are positive, ranging from 1.6 to 5.8 s. The sizes of the circles of the labels are proportional to the amplitudes of the anomalies. (B) Seismograms of the polar paths marked in A. The traces are aligned with AB. The predicted DF arrivals (with ellipticity corrections) are marked.

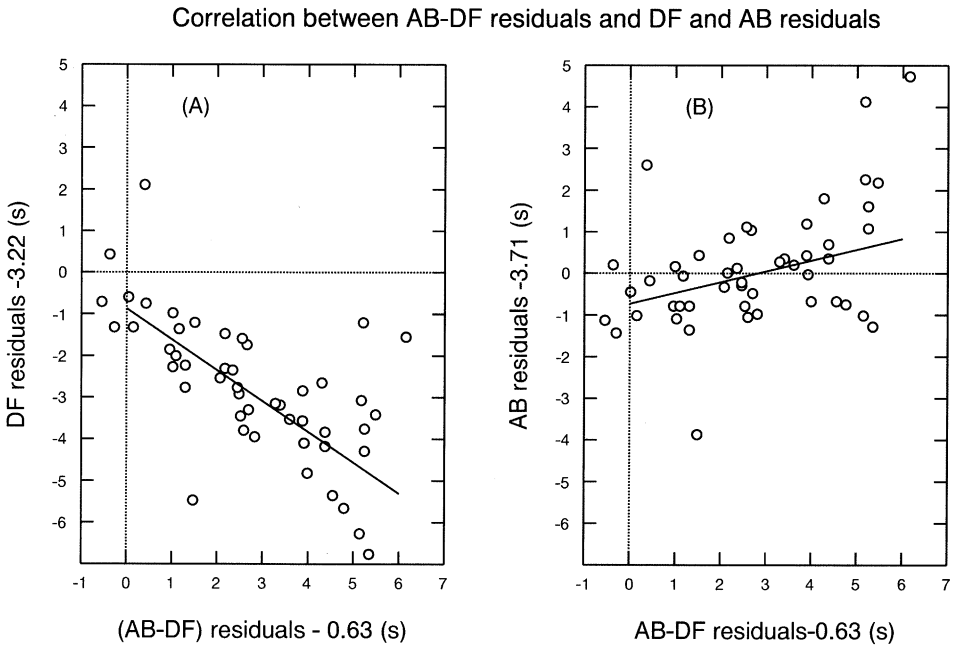

Fig. 6. Observed AB–DF residuals vs. DF residuals (A) and AB residuals (B) for the polar paths. The lines are linear regressions excluding the four outliers. The AB–DF, DF, and AB residuals are shifted by the averages of equatorial paths with $\xi = 60–90°$, 0.63 s, 3.22 s, and 3.71 s, respectively. The DF residuals explain most of the AB–DF anomalies (from 0 to about 6 s) and correlate well with the AB–DF residuals.

[30,31], respectively, the anisotropy at the innermost 700 km of the inner core is about 3.0%.

Fig. 4 shows some examples of polar path data, sampling different parts of the world. The ray angles (ξ) range from 5° (path 1) to 36° (path 16). Fig. 4A is a map of the ray paths. We can see that although the locations of events and stations are limited to a few isolated areas, the ray paths cover all the longitudes quite well. This is a key advantage of using antipodal data as we discussed previously. The quality of all seismograms for these polar paths is excellent (Fig. 4B). When the seismograms are aligned with AB arrival times, the DF arrivals are clearly earlier than the predicted times. The AB–DF residuals of these paths range from 1.6 to 5.8 s.

To examine the lateral variation of the anisotropy in the central inner core, we plot all the polar path data at DF ray turning points in the inner core in a map view (Fig. 5A) and at the radii and longitudes of the DF turning points (Fig. 5B). The paths sampling the deepest part of the inner core do not show hemispherical pattern, but there is some indication of weaker anisotropy in the eastern hemisphere at shallower depths of the central inner core. At the sampling radii of about 300–400 km, the residuals at sampling longitudes of 20–200° appear to be smaller and all the negative residuals are in these longitudes.

3.2. *Effect of mantle structure*

As we mentioned before, AB–DF differential times can be affected by lowermost mantle structure, which has been proven to be very heterogeneous [38–42]. Differential AB–DF times at antipodal distances provide an ideal test for the degree of influence of mantle heterogeneity on the inference of inner core anisotropy using PKP differential times because of the greatest separation (by a few thousand kilometers) of the AB and DF rays in the lowermost mantle.

So could most of the observed AB–DF anomalies of the polar paths discussed above come from mantle heterogeneity? Two observations from the

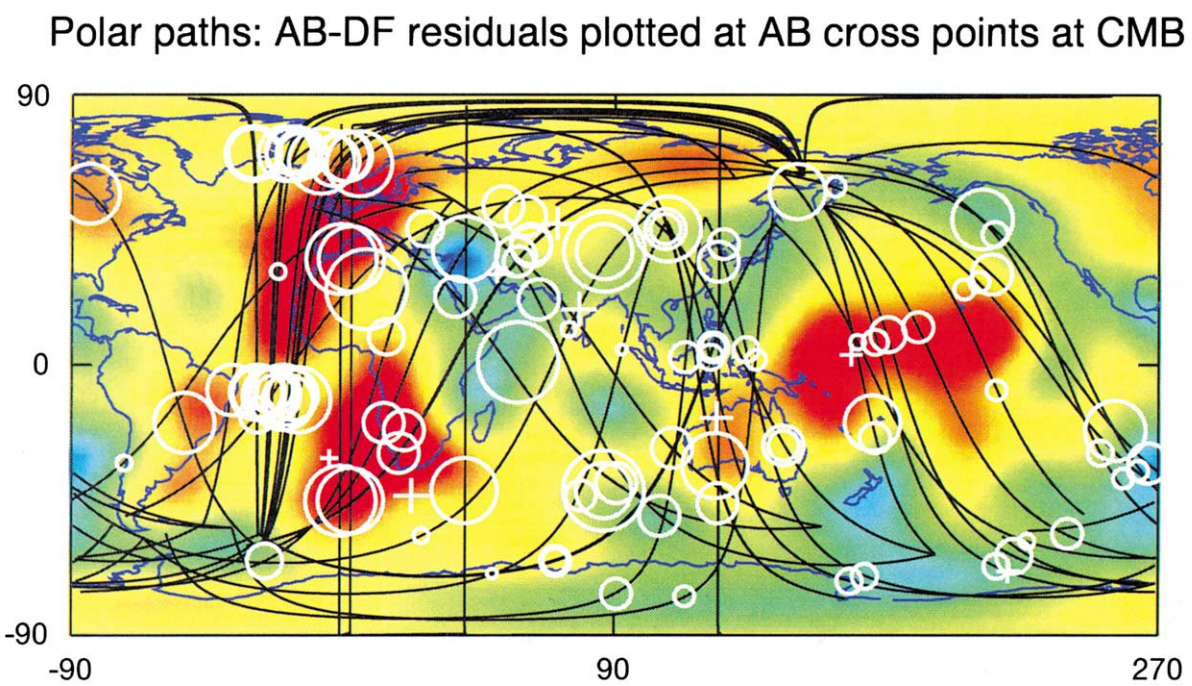

Fig. 7. Observed AB–DF residuals of the polar paths plotted at the cross points of the AB rays with the CMB. On the background is SH12WM13 model [38] at the CMB. Note some of the large anomalies occur at the fast velocity region (blue) and some of the small anomalies occur at the low velocity region (red).

previous sections argue against it. (1) The AB–DF residuals appear to be anti-correlated with the DF residuals and do not appear to have obvious correlation with the AB residuals (Fig. 3). (2) The AB rays of the polar paths sample all the longitudes and latitudes (Fig. 2) and thus should be affected by both slow and fast mantle anomalies. The regions sampled by the AB rays of the polar paths are well sampled by the AB rays of the equatorial paths (Fig. 2). Yet all the AB–DF residuals of the polar paths are larger than the average of the residuals of the equatorial paths (Fig. 3). We explore this issue in details below.

Fig. 6 compares the AB–DF residuals with the DF residuals (A) and the AB residuals (B) of those polar paths (a total of 48) that have simultaneous measurements of absolute and differential times. The residuals are plotted relative to the averages of equatorial paths with $\xi = 60$–$90°$, i.e. the AB–DF, DF, and AB residuals of the polar paths are shifted by 0.63 s, 3.22 s, and 3.71 s, respectively. The lines are linear regressions excluding the four outliers. The DF residuals explain most of the AB–DF anomalies (from 0 to 6 s), and correlate well with the AB–DF residuals. The slopes of linear regressions with and without the four outliers are -0.62 ± 0.10 and -0.74 ± 0.07, respectively. The correlation coefficients between the DF residuals and the AB–DF residuals are -0.90 and -0.96 with and without the four outliers, respectively. The negative sign indicates anti-correlation. The AB residuals, on the other hand, scatter around 0 s. The slopes of linear regressions of AB–DF residuals on AB residuals are 0.38 ± 0.10 and 0.26 ± 0.07 with and without the four outliers, respectively. The correlation coefficients between the AB residuals and the AB–DF residuals are 0.34 and 0.23 with and without the four outliers, respectively. Thus, although there may be some contribution to the AB–DF anomalies from the AB phase, most of the AB–DF anomalies of the polar paths come from the DF phase.

We now examine in detail the effect of mantle

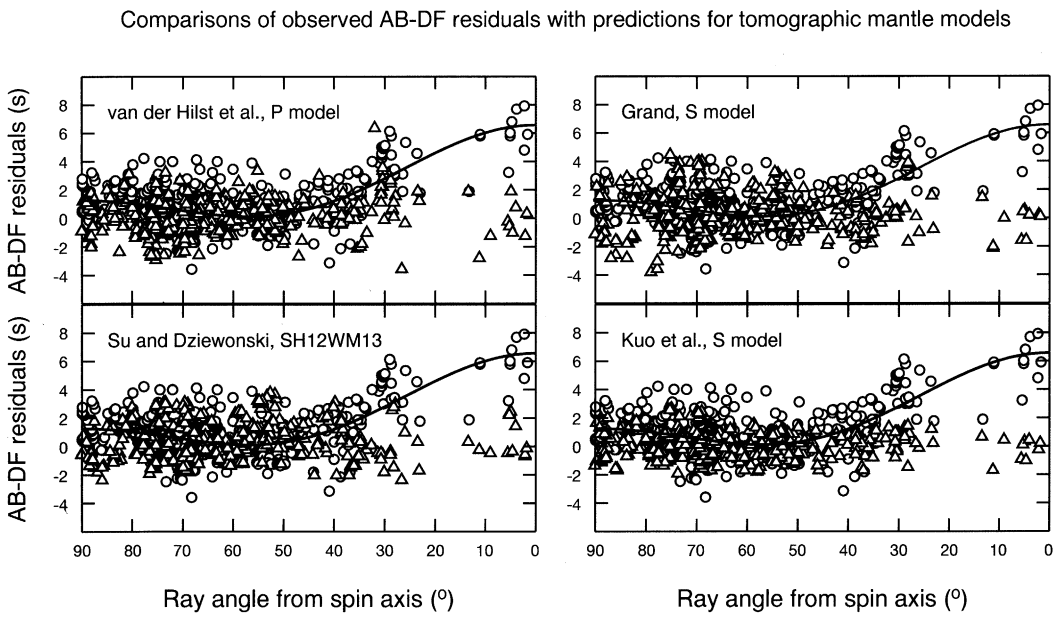

Fig. 8. Comparisons of observed AB–DF times (circles) with predictions (triangles) for four tomographic mantle models: P model by van der Hilst et al. [39] (amplified by a factor of 3) and three S models: Grand [40], Su and Dziewonski [38] (SH12WM13), and Kuo et al. [42]. Note the mantle predictions cannot explain the observed large positive anomalies in NS directions.

structure on the AB–DF residuals by comparing with predictions for mantle tomographic models. Fig. 7 shows the polar paths and the AB cross points at the CMB, plotted on top of S tomographic model SH12WM13 [38] at the CMB. Note that the observed large AB–DF anomalies lie in both slow and fast areas of the CMB. A slow anomaly slows down the AB phase, increasing the AB–DF time; a fast anomaly speeds up the AB phase, decreasing the AB–DF time. But in Fig. 7, some of the large AB–DF residuals lie in the area with fast velocity anomalies, such as in the circum-Pacific rim and north-eastern Africa. In the central Pacific with large slow velocity anomaly ('the central Pacific plume'), the AB–DF residuals are small. These observations suggest that it is difficult to explain the AB–DF anomalies of the polar paths with mantle heterogeneity.

Direct comparisons of the observed AB–DF residuals with predictions for four tomographic models are shown in Fig. 8. The mantle predictions are calculated by tracing the ray paths through the tomographic models. The four tomographic models are the P model from van der Hilst et al. [39] and the S models from Grand [40], Su and Dziewonski [38] (SH12WM13), and Kuo et al. [42]. The Grand model used is the most recent version. The Kuo et al. model was an inversion of the lowermost mantle S heterogeneity from differential S-SKS times. All the other models are inversions of the whole mantle. In calculating the PKP travel time perturbations for the S tomographic models, we map S perturbations to P perturbations with an S to P scaling factor of 1 (i.e. $\mathrm{dln}(V_s)/\mathrm{dln}(V_p) = 1$).

The perturbations for the van der Hilst et al. model have been amplified three times since the perturbations are too small, compared with the scatter of the data. This assumes that the P model underestimates the level of heterogeneity, particularly in the lowermost mantle, which has been suggested [43]. We see that except for a couple of points of the mantle predictions around ray angle $\xi = 30°$, none of the models can explain the large AB–DF residuals of the polar paths (Fig. 8). The averages of the model predictions for the polar paths are about the same as those for equatorial paths.

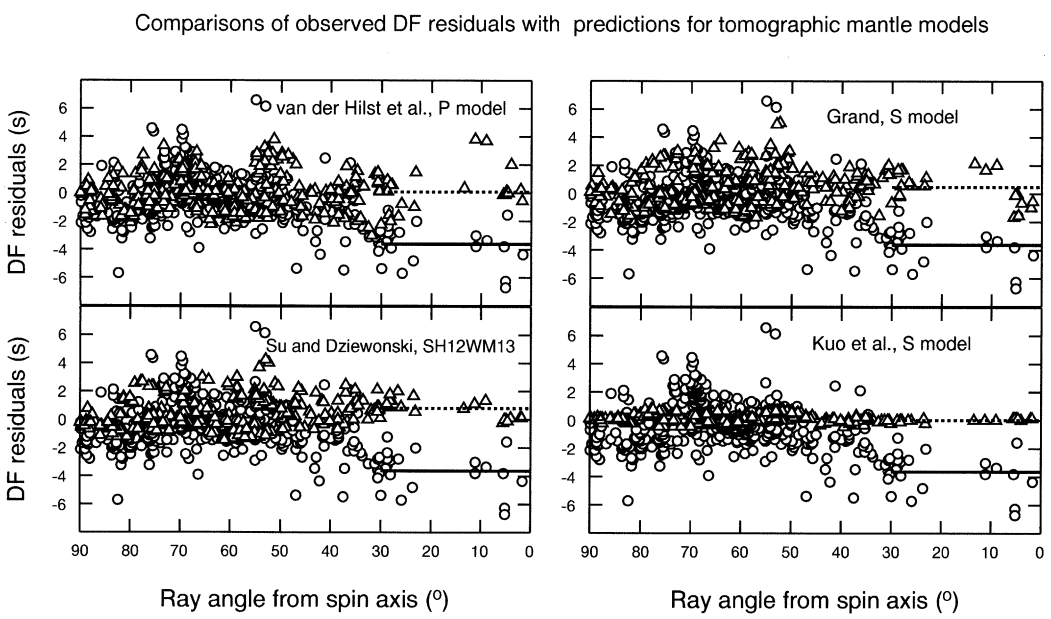

Fig. 9. Same as Fig. 8, but for observed DF residuals (circles) and mantle predictions (triangles). The residuals and predictions have been shifted by the corresponding averages for the equatorial paths with $\xi > 60°$. The averages of the values for the polar paths with $\xi < 30°$ are marked by the solid lines (observations) and the dashed lines (predictions). Note the mantle predictions do no show large negative anomalies at NS directions as in the data.

Similar to Fig. 8, Fig. 9 shows direct comparisons of the observed DF residuals with predictions for the four tomographic models. Since our interest is the anomalous residuals of the polar paths relative to those of the equatorial paths, we shift the data residuals and the mantle predictions by the corresponding averages for the equatorial paths at $\xi = 60$–$90°$. Fig. 9 shows that the mantle models cannot explain the anomalously fast DF anomalies of the polar paths. The average of the observed DF residuals for the polar paths at $\xi = 0$–$30°$ is about 4 s faster than the corresponding averages of the mantle predictions. In fact, contrary to the observed residuals, the averages of the mantle predictions at $\xi = 0$–$30°$ are slightly (by up to 0.8 s) slower than the averages of the mantle predictions for the equatorial paths at $\xi = 60$–$90°$ (i.e. the zero baseline).

Thus most of the observed AB–DF anomalies of the polar paths cannot come from mantle heterogeneity. Can the mantle models explain some of the observed AB–DF residuals? We consider the equatorial and the polar paths separately. The majority of our data are from equatorial paths, which are not sensitive to the inner core anisotropy. We first examine the effect of a mantle model by subtracting scaled mantle predictions from the equatorial data. After applying different scaling factors from 0 to 3 to the mantle predictions, we select the best scaling factor that reduces the variance of the data the most. Fig. 10 shows the observed AB–DF residuals corrected by various mantle models with the best scaling factors. The van der Hilst et al. P model achieves 13% variance reduction of the equatorial data with the best scaling factor of 1.1.

For the Grand S model, we divide the mantle into two parts: the lowermost 300 km with a variable scaling factor and the rest of the mantle with a fixed scaling factor of 0.5 (i.e. the S to P conversion $d\ln(V_s)/d\ln(V_p) = 2$). This is motivated by the recent work of Bréger et al. [34]. They found that the observed trends in the AB–DF times from equatorial paths and a large part of the AB–DF signal from polar paths could be explained by tomographic mantle models, when the amplitudes of the models at the lowermost mantle are increased and the ultra-low velocity

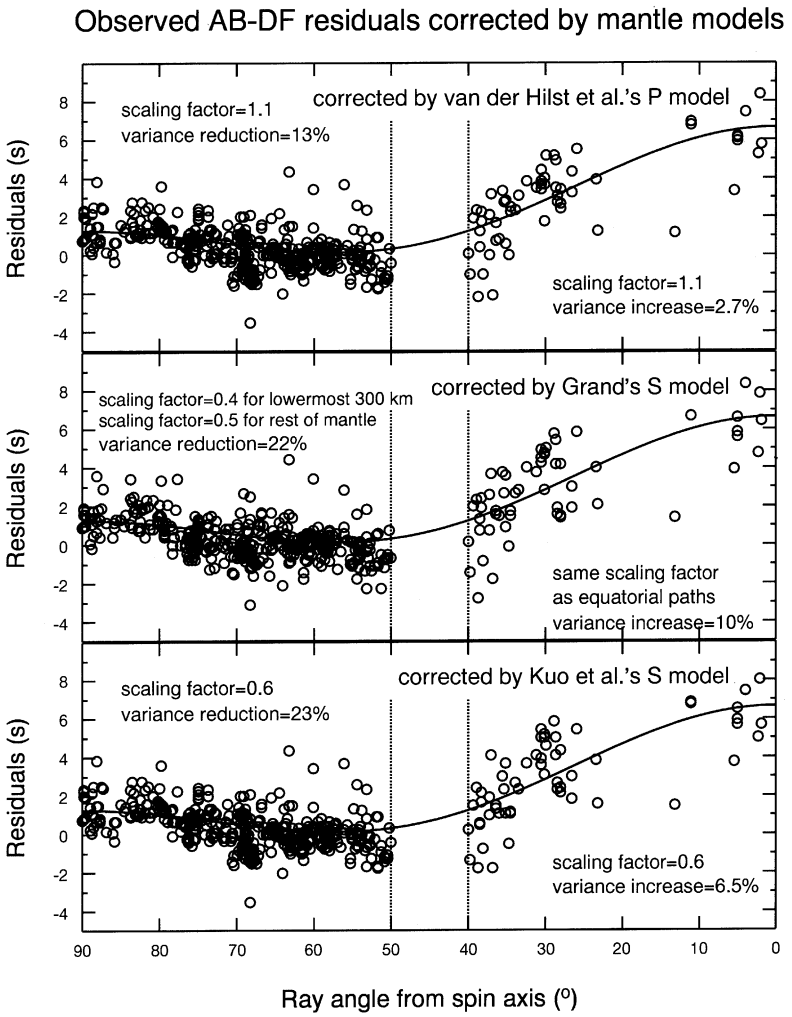

Fig. 10. Observed AB–DF residuals corrected by mantle models of van der Hilst et al. [39] (top panel), Grand [40] (middle panel), and Kuo et al. [42] (bottom panel). The solid lines are from the uniform anisotropy model of this study. The mantle predictions are scaled before the corrections to achieve the smallest variances of the corrected residuals for the equatorial paths ($\xi > 50°$). Note mantle corrections increase the data variances for the polar paths ($\xi < 40°$) when the best scaling factors for the equatorial paths are used.

zones at the base of the mantle that have been identified are included. We found that the Grand model reduces the variance of the equatorial data by 22% with the best scaling factor of 0.4 for the lowermost 300 km. The Kuo et al. model achieves 23% variance reduction of the equatorial data with the best scaling factor of 0.6. These results suggest that current mantle models can explain part of the AB–DF anomalies of the equatorial paths.

However, mantle models explain little of the large AB–DF anomalies of the polar paths (Fig. 10). When the Grand or Kuo et al. model is applied, no matter what scaling factor is used, the data variance increases. For the van der Hilst et al. model, we do achieve some but negligible (less than 0.5%) variance reduction when the scaling factor is less than 0.6; when the scaling factor increases, the variance increases steadily. If we apply mantle corrections with the same scaling

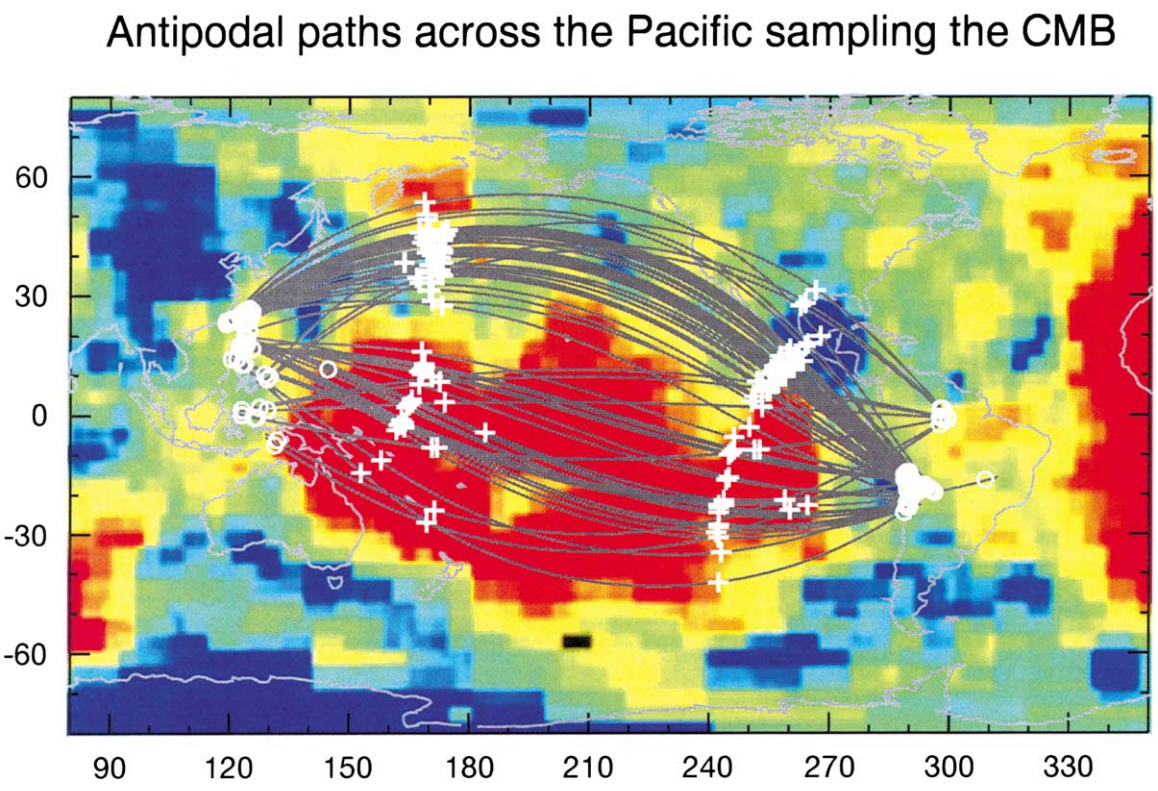

Fig. 11. Ray paths at near antipodal distances from earthquakes in the west Pacific to stations in South America. On the background is Grand's most recent S model at the CMB. The cross points of the DF and AB rays with the CMB are marked with circles and crosses, respectively. Note the rays sweep across the great slow anomaly (red color) at the CMB beneath the central Pacific.

factors as those for the equatorial paths, the variances of the polar data increase by 3%, 10%, and 7%, for the van der Hilst et al., Grand, and Kuo et al. models, respectively.

4. Equatorial paths from west Pacific to South America

Among all the equatorial paths, a data set from earthquakes in the west Pacific to stations in South America (Fig. 11) appears very interesting. Over a half of the data are from 1994 PASSCAL experiment BANJO (S.L. Beck, T.C. Wallace, P. Silver, Principal Investigators) and 1996–1997 PASSCAL experiment APVC (G. Zandt, Principal Investigator). The rest of the data are from permanent stations of global digital seismic networks. The data provide a good coverage of the central Pacific plume with rays sweeping from the south Pacific to the north Pacific. The observed AB–DF residuals shows a distinct trend: they increase slightly from back azimuth 230° to 260° and then decrease sharply by about 4 s over a 60° azimuth range (from back azimuth 250° to 310°) (Fig. 12). We see a similar azimuthal variation in the AB residuals but only a slight increase in DF residuals over the same azimuth range. This suggests that the AB–DF variation comes from the AB rays sampling the central Pacific.

We calculated travel time perturbations along these paths for four mantle models (van der Hilst et al.'s, SH12WM13, Grand's, and Kuo et al.'s) (Fig. 13). All the predictions for these models reveal azimuthal trends strikingly similar to the trend in the observed data. The predicted AB–DF residuals correlate well with the observed data. The cross-correlation coefficients are 0.75.

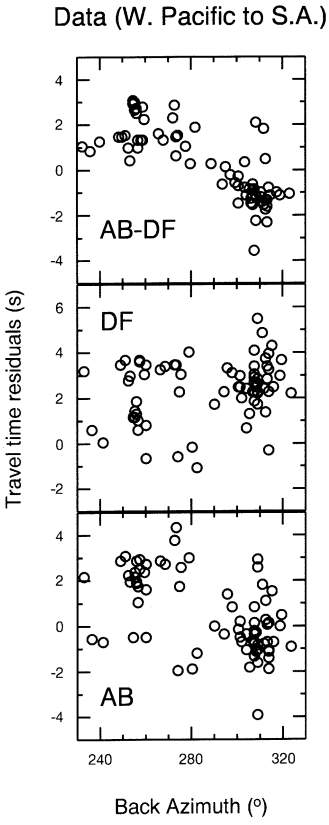

Fig. 12. Residuals of AB–DF (top), DF (middle), and AB (bottom) travel times from earthquakes in the west Pacific to stations in South America (see ray paths in Fig. 11), plotted as a function of back azimuth. Note a very sharp decrease in the AB–DF residuals by about 4 s over a 60° azimuth range and a similar decrease in the AB residuals, suggesting that the AB–DF variation comes from the AB rays sampling the central Pacific.

0.69, 0.81, and 0.81 for van der Hilst et al.'s model, SH12WM13, and Grand's and Kuo et al.'s models, respectively. If we correct the observed AB–DF residuals for the mantle predictions with various scaling factors, the variance reductions are 56%, 47%, 67%, and 61% with the best scaling factors of 3.3, 0.7, 0.5, and 1.0 for van der Hilst et al.'s model, SH12WM13, and Grand's and Kuo et al.'s models, respectively.

The predicted DF perturbations show no change or a slight increase with azimuths and the predicted AB perturbations show azimuthal trends very similar to the predicted AB–DF perturbations. This agrees with the observed AB–DF, DF, and AB residuals, suggesting that the observed AB–DF azimuthal variation indeed comes from the AB paths. Looking closely at the ray paths (Fig. 11), we can see that the azimuthal change occurs when the AB paths sweep across the great slow anomaly in the central Pacific at the CMB. At back azimuth around 240°, the AB rays sample the southern edges of the slow anomaly. At back azimuth around 270°, the AB rays cross the very low velocity zones at both the event and station sides, slowing down the AB arrivals and thus increasing the AB–DF times. As the back azimuth increases, the AB ray paths miss the slow anomaly and sample the normal region underneath the north Pacific and then the fast anomalies underneath the Aleutian and central America around the Pacific rim, so that the AB arrivals become normal and then fast, producing the decreasing trend in the AB–DF times.

5. Conclusion and discussion

We gathered and analyzed systematically differential and absolute AB and DF travel times for both polar and equatorial paths at near antipodal distances. We observed large AB–DF anomalies (up to 8 s) for the polar paths. We conclude that most of the polar path anomalies come from the inner core based on the following results. (1) The regions sampled by the AB rays of the polar paths are well sampled by the AB rays of the equatorial paths, and yet all the AB–DF residuals of the polar paths are larger than the average residuals of the equatorial paths. (2) The DF residuals explain most of the AB–DF anomalies and they anti-correlate strongly with the AB–DF residuals. The AB residuals, on the other hand, scatter around 0 s, and they correlate weakly with the AB–DF residuals. Thus, most of the polar AB–DF anomalies are from the DF rays. (3) We compared the observed differential and absolute travel times with predictions for various mantle tomographic models. The mantle models can explain part of the overall observed AB–DF residuals of the equatorial paths and can explain most of the AB–DF residuals of the equatorial

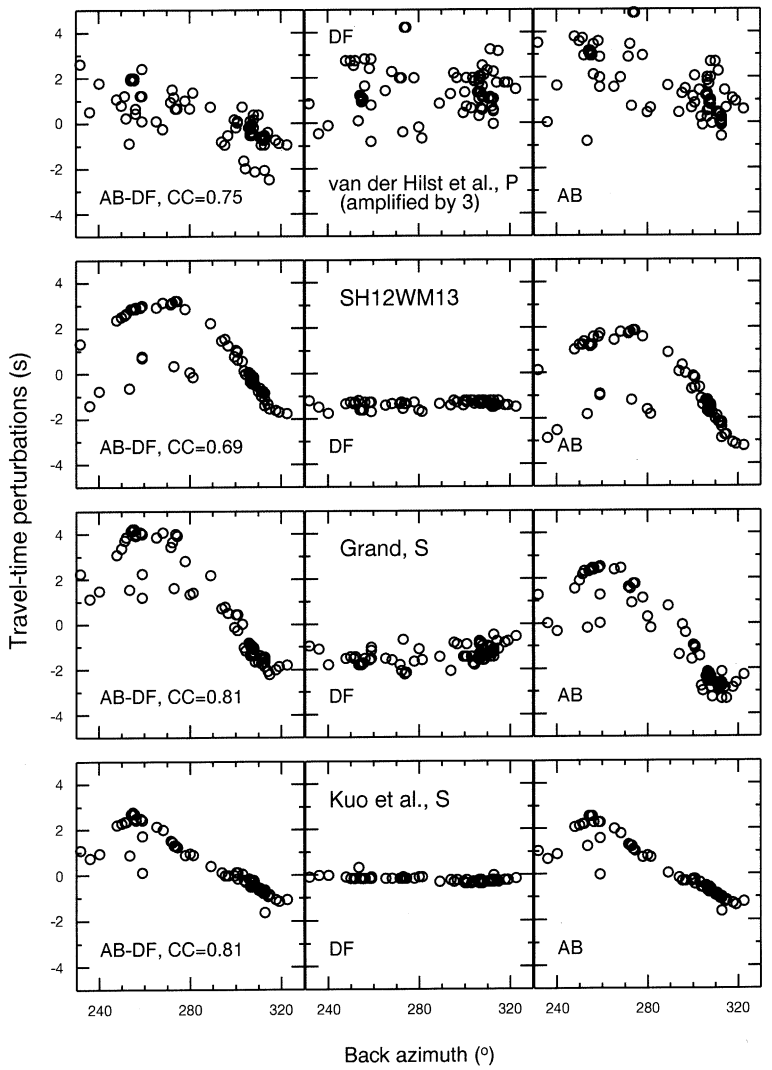

Fig. 13. Predictions of AB–DF (left column), DF residuals (middle column), and AB residuals (right column) for tomographic models by van der Hilst et al. (amplified by a factor of 3), Su and Dziewonski (SH12WM13), Grand, and Kuo et al. All the models predict the azimuthal trend as in the observed AB–DF differential and AB absolute times well. Grand's and Kuo et al.'s models predict the azimuthal variation the best with cross-correlation coefficients (CC) of 0.81, suggesting P and S anomalies are well correlated for this region.

paths sampling the central Pacific. But the same mantle models cannot explain the large differential AB–DF residuals or absolute DF residuals of polar paths at all.

Assuming a uniform cylindrical anisotropy model with the fast axis in the NS direction, the average inner core anisotropy amplitude is about 2.5%. If we take into account the isotropy at the upper inner core as suggested by previous studies, the degree of anisotropy in central inner core would be higher.

We also observed a steep azimuthal variation in AB–DF times (about 4 s in a 60° azimuth range) from earthquakes in the west Pacific recorded at South American stations, sampling the central Pacific plume at the CMB. Current tomographic models can explain the general azimuthal trend. The azimuthal variation arises when the AB rays

pass through the low velocity anomalies at CMB in central Pacific. Among the mantle models we considered, only van der Hilst et al.'s model is a P velocity model while the other three are S models. The high correlation coefficients between these S models and the PKP data seem to indicate that in this region, the P and S velocities correlate very well, leading us to speculate that the central Pacific slow anomaly may be of thermal origin. The result also shows the potential of using PKP data across the Pacific, which are abundant, to image the fine structure of the central Pacific anomaly.

Acknowledgements

Data for this paper are from global networks and PASSCAL experiments at the IRIS data center and WWSSN film chip library at Lamont-Doherty Earth Observatory, and from A. Souriau and B. Romanowicz. We thank Steve Grand, Ban-Yuan Kuo for sending us their most recent tomographic models and Weijia Su and Rob van der Hilst for their models. We thank Thorne Lay and an anonymous reviewer for their very positive and constructive comments and Jay Bass for detailed review of the early draft of the paper. This paper was supported by NSF Grant EAR 01-06544.*[SK]*

References

[1] A. Morelli, A.M. Dziewonski, J.H. Woodhouse, Anisotropy of the inner core inferred from PKIKP travel times, Geophys. Res. Lett. 13 (1986) 1545–1548.
[2] J.H. Woodhouse, D. Giardini, X.-D. Li, Evidence for inner core anisotropy from free oscillations, Geophys. Res. Lett. 13 (1986) 1549–1552.
[3] X.D. Song, Anisotropy of the earth's inner core, Rev. Geophys. 35 (1997) 297–313.
[4] K.C. Creager, Inner core anisotropy and rotation, in: S. Karato, A.M. Forte, R.C. Liebermann, G. Masters, L. Stixrude (Eds.), Earth's Deep Interior: Mineral Physics and Tomography From the Atomic to the Global Scale (Geophyiscal Monograph 117), Am. Geophys. Union, Washington, DC, 2000, pp. 89–114.
[5] X.D. Song, Three-dimensional inner core structure and differential rotation of inner core, AGU Monogr. (2001) submitted.
[6] J. Tromp, Inner-core anisotropy and rotation, Annu. Rev. Earth Planet. Sci. 29 (2001) 47–69.
[7] J.M. Brown, R.G. McQueen, Phase-transitions, gruneisen-parameter, and elasticity for shocked iron between 77-GPA and 400-GPA, Geophys. J. R. Astron. Soc. 91 (1986) 7485–7494.
[8] O.L. Anderson, Properties of iron at the Earth's core conditions, Geophys. J. R. Astron. Soc. 84 (1986) 561–579.
[9] A. Jephcoat, P. Olson, Is the inner core of the Earth pure iron?, Nature 325 (1987) 332–335.
[10] C.M. Sayers, Seismic anisotropy of the inner core, Geophys. Res. Lett. 16 (1989) 267–270.
[11] L. Stixrude, R.E. Cohen, High-pressure elasticity of iron and anisotropy of Earth's inner core, Science 267 (1995) 1972–1975.
[12] G. Steinle-Neumann, L. Stixrude, R.E. Cohen, O. Gulseren, Elasticity of iron at the temperature of the Earth's inner core, Nature 413 (2001) 57–60.
[13] R. Jeanloz, H.R. Wenk, Convection and anisotropy of the inner core, Geophys. Res. Lett. 15 (1988) 72–75.
[14] S. Yoshida, I. Sumita, M. Kumazawa, Growth-model of the inner core coupled with the outer core dynamics and the resulting elastic anisotropy, J. Geophys. Res. 101 (1996) 28085–28103.
[15] S. Karato, Seismic anisotropy of the Earth's inner core resulting from flow induced by Maxwell stresses, Nature 402 (1999) 871–873.
[16] S. Karato, Inner core anisotropy due to the magnetic field-induced preferred orientation of iron, Science 262 (1993) 1708–1711.
[17] M.I. Bergman, Measurements of elastic anisotropy due to solidification texturing and the implications for the Earth's inner core, Nature 389 (1997) 60–63.
[18] X.D. Song, P.G. Richards, Observational evidence for differential rotation of the Earth's inner core, Nature 382 (1996) 221–224.
[19] K.C. Creager, Inner core rotation rate from small-scale heterogeneity and time-varying travel times, Science 278 (1997) 1284–1288.
[20] X.D. Song, Joint inversion for inner core rotation, inner core anisotropy, and mantle heterogeneity, J. Geophys. Res. 105 (2000) 7931–7943.
[21] P.M. Shearer, Constraints on inner core anisotropy from PKP(DF) travel-times, J. Geophys. Res. 99 (1994) 19647–19659.
[22] X.D. Song, D.V. Helmberger, Depth dependence of anisotropy of Earth's inner core, J. Geophys. Res. 100 (1995) 9805–9816.
[23] X.D. Song, D.V. Helmberger, Seismic evidence for an inner core transition zone, Science 282 (1998) 924–927.
[24] F.L. Niu, L.X. Wen, Hemispherical variations in seismic velocity at the top of the Earth's inner core, Nature 410 (2001) 1081–1084.
[25] A. Ouzounis, K.C. Creager, Isotropy overlying anisotropy at the top of the inner core, Geophys. Res. Lett. 28 (2001) 4331–4334.

[26] L. Vinnik, B. Romanowicz, L. Bréger, Anisotropy in the center of the inner core, Geophys. Res. Lett. 21 (1994) 1671–1674.
[27] X.D. Song, Anisotropy in central part of inner core, J. Geophys. Res. 101 (1996) 16089–16097.
[28] X.D. Song, X.X. Xu, Inner core transition zone and anomalous PKP(DF) waveforms from north-south paths, Geophys. Res. Lett. 29 (2002) 10.1029/2001GL013822.
[29] R. Garcia, A. Souriau, Inner core anisotropy and heterogeneity level, Geophys. Res. Lett. 27 (2000) 3121–3124.
[30] S. Tanaka, H. Hamaguchi, Degree one heterogeneity and hemispherical variation of anisotropy in the inner core from PKP(BC)-PKP(DF) times, J. Geophys. Res. 102 (1997) 2925–2938.
[31] K.C. Creager, Large-scale variations in inner core anisotropy, J. Geophys. Res. 104 (1999) 23127–23139.
[32] J. Tromp, Support for anisotropy of the Earth's inner core from free oscillations, Nature 366 (1993) 678–681.
[33] L. Bréger, B. Romanowicz, H. Tkalcic, PKP(BC-DF) travel time residuals and short scale heterogeneity in the deep earth, Geophys. Res. Lett. 26 (1999) 3169–3172.
[34] L. Bréger, H. Tkalcic, B. Romanowicz, The effect of D″ on PKP(AB–DF) travel time residuals and possible implications for inner core structure, Earth Planet. Sci. Lett. 175 (2000) 133–143.
[35] G. Poupinet, A. Souriau, L. Jenatton, A test on the Earth's core-mantle boundary structure with antipodal data: example of Fiji-Tonga earthquakes recorded in Tamanrasset, Algeria, Geophys. J. Int. 113 (1993) 684–692.
[36] A.M. Dziewonski, D.L. Anderson, Preliminary reference Earth model, Phys. Earth Planet. Inter. 25 (1981) 297–356.
[37] X.D. Song, D.V. Helmberger, Anisotropy of Earth's inner core, Geophys. Res. Lett. 20 (1993) 2591–2594.
[38] W.J. Su, A.M. Dziewonski, Degree 12 model of shear velocity heterogeneity in the mantle, J. Geophys. Res. 99 (1994) 6945–6980.
[39] R.D. Van der Hilst, S. Widiyantoro, E.R. Engdahl, Evidence for deep mantle circulation from global tomography, Nature 386 (1997) 578–584.
[40] S.P. Grand, R.D. van der Hilst, S. Widiyantoro, Global seismic tomography a snapshot of convection in the Earth, GSA Today 7 (1997) 1–7.
[41] E.J. Garnero, D.V. Helmberger, Seismic detection of a thin laterally varying boundary layer at the base of the mantle beneath the central-Pacific, Geophys. Res. Lett. 9 (1996) 977–980.
[42] B.-Y. Kuo, E.J. Garnero, T. Lay, Tomographic inversion of S-SKS times for shear velocity heterogeneity in D″: Degree 12 and hybrid models, J. Geophys. Res. 105 (2000) 28139–28157.
[43] X.D. Song, D.V. Helmberger, PKP differential travel times: Implications from three-dimensional lower mantle structure, Geophys. Res. Lett. 24 (1997) 1863–1866.